Journal of Orthopaedic Translation 50 (2025) 14–29

Contents lists available at ScienceDirect

Journal of Orthopaedic Translation

journal homepage: www.journals.elsevier.com/journal-of-orthopaedic-translation

Original Article

# OGT mediated HDAC5 O-GlcNAcylation promotes osteogenesis by regulating the homeostasis of epigenetic modifications and proteolysis

Yu Du [a,1], Xiang Gao [a,b,c,1], Jianqiang Chen [b], Xinxin Chen [d], Hang Liu [a,c], Wenge He [c,e], Lu Liu [c], Yue Jiang [c], Baicheng He [c], Zhongliang Deng [a], Chao Liang [d,f,g,**], Fengjin Guo [a,b,2,*]

[a] Department of Orthopedics, The Second Affiliated Hospital of Chongqing Medical University, Chongqing Medical University, Chongqing, China
[b] State Key Laboratory of Ultrasound in Medicine and Engineering, School of Basic Medical Sciences, The Second Affiliated Hospital of Chongqing Medical University, Chongqing Medical University, Chongqing, China
[c] Department of Pharmacology, School of Pharmacy, Chongqing Medical University, Chongqing, China
[d] Department of Systems Biology, School of Life Sciences, Southern University of Science and Technology, Shenzhen, China
[e] Department of Orthopaedics, The First Affiliated Hospital of Chongqing Medical University, Chongqing Medical University, Chongqing, China
[f] Institute of Integrated Bioinfomedicine and Translational Science (IBTS), School of Chinese Medicine, Hong Kong Baptist University, Hong Kong SAR, China
[g] State Key Laboratory of Proteomics, National Center for Protein Sciences (Beijing), Beijing Institute of Lifeomics, Beijing, China

ARTICLE INFO

*Keywords:*
HDAC5
O-GlcNAcylation
OGT
Osteogenesis
Proteolysis

ABSTRACT

*Background:* O-GlcNAc transferase (OGT) is responsible for attaching O-linked N-acetylglucosamine (O-GlcNAc) to proteins, regulating diverse cellular processes ranging from transcription and translation to signaling and metabolism. This study focuses on the role and mechanisms of OGT in osteogenesis.

*Materials and methods:* We found that OGT is downregulated in osteoporosis by bioinformatics analysis, determined its role in osteogenic differentiation by using OGT inhibitors (or OGA inhibitors) as well as conditional knockout OGT mice in *vitro* and in *vivo*, and explored and specific mechanisms by quantitative proteomic analysis and RNA-seq, qRT-PCR, western blotting, immunofluorescence, H&E, ALP, ARS, Masson staining, IHC, micro CT, etc.

*Results:* we revealed that OGT positively influenced osteogenesis and osteoblast differentiation in *vitro* as well as ovariectomy (OVX) mice in *vivo*. Consistently, mice with conditionally depleted OGT exhibited a reduction in bone mass, while O-GlcNAcylation enhancer could partially recover bone mass in ovariectomy (OVX) mice. Mechanistically, quantitative proteomic analysis and high-throughput RNAseq further reveals that HDAC5 is one of the endogenous O-GlcNAcylation substrates, and O-GlcNAcylation of HDAC5 on Thr934 promotes its translocation to lysosomes and subsequent degradation, thus, elevating the O-GlcNAcylation level of HDAC5 leads to its cytoplasmic cleavage, consequently diminished its nuclear entry and enhanced DNA transcription. The OGT-mediated O-GlcNAcylation of HDAC5 modulates the balance between its cytoplasmic proteolysis and nuclear entry, thereby impacting the Notch signaling pathway and DNA epigenetic modifications then playing a role in osteogenesis.

*Conclusion:* OGT is a regulator that promotes osteoblast differentiation and bone regeneration. Additionally, it highlights the critical function of HDAC5 O-GlcNAcylation in controlling epigenetics. This study offers fresh perspectives on osteogenesis and O-GlcNAcylation, proposing that the OGT-mediated O-GlcNAcylation of HDAC5 could be a promising target for osteoporosis treatment.

*The translational potential of this article:* On one side, OGT might potentially be used as a new biomarker for clinical diagnosis of osteoporosis (OP) in the future. On the other side, small molecule inhibitors of HDAC5, a glycosylation substrate of OGT, or OGT agonists such as silymarin, could all potentially serve as therapeutic targets for the prevention or treatment of OP in the future.

* Corresponding author. State Key Laboratory of Ultrasound in Medicine and Engineering, School of Basic Medical Sciences, The Second Affiliated Hospital of Chongqing Medical University, Chongqing Medical University, Chongqing, China.
** Corresponding author. Department of Systems Biology, School of Life Sciences, Southern University of Science and Technology, Shenzhen, China.
*E-mail addresses:* liangc@sustech.edu.cn (C. Liang), guo.fengjin@cqmu.edu.cn (F. Guo).
[1] These authors contribute equally.
[2] Lead contact.

https://doi.org/10.1016/j.jot.2024.10.004
Received 24 June 2024; Received in revised form 19 September 2024; Accepted 17 October 2024

## 1. Introduction

Osteoporosis (OP) is a prevalent bone disease that is characterized by a reduction in bone mass, damage to bone microstructure, and an increase in bone fragility [1], and it is found in an estimated 200 million people worldwide, 50 % women and 20 % men aged over 50 years will suffer an osteoporotic fracture in their lifetime [2]. The maintenance of bone homeostasis depends on the balance between osteoclast-induced bone resorption and osteoblast-triggered bone formation. Decreased osteoblast differentiation and(or)increased osteoclast differentiation will result in osteoporosis. It is well known that bone marrow stem cells (BMSCs) are non-hematopoietic bone marrow stromal cells with the ability to differentiate into a variety of cell types, including osteoblasts [3]. And stimulating osteogenic differentiation of BMSC represents a primary approach for treating osteoporosis [4–6]. Further studies are essential to understand the osteogenic mechanisms of MSCs and to identify novel therapeutic targets for OP.

O-GlcNAc, as a novel epigenetic mark, participates in the dynamic cycling of histones, playing a crucial role in regulating chromatin remodeling and gene expression. The cycling of O-GlcNAc is catalyzed by two highly conserved enzymes, O-GlcNAc transferase (OGT), responsible to attach single O-linked N-acetylglucosamine (*O*-GlcNAc) moieties to serine and threonine [7]. And β-N-acetylglucosaminidase (O-GlcNAcase, OGA), which hydrolyzes it. O-GlcNAcylaction is one of the common post-translational modification and is widely distributed in the nucleus and cytoplasm [8,9], involved in multiple cellular processes ranging from transcription and translation to signal transduction and metabolism [10,11]. On one side, OGT and O-GlcNAcylation regulate the activity of various co-repressors, promoting chromatin condensation and inhibiting gene transcription. On the other side, O-GlcNAcylation may also facilitate DNA demethylation by interacting with members of the TET family of proteins, promoting chromatin relaxation and enhancing gene transcription. Additionally, O-GlcNAcylation regulates other translation modifications that define the histone code by modulating the activity of several methyltransferases, including MLL5, CARM1, and HCF1 etc [12–14]. Several recent studies have consistently indicated that OGT and OGT-mediated O-GlcNAcylation are positively related to osteogenesis [15,16].

Histone deacetylase 5 (HDAC5) is a member of the histone deacetylase (HDACs) family. HDACs facilitate the removal of acetyl groups from histones, facilitating the binding of histones to DNA and restricting access to the DNA once again. HDAC5 was reported that it directly binds to MEF2 at the promoter regions of muscle genes, reducing acetylation levels on histone tails [17].During induced differentiation, HDAC5 can be released from MEF2 through activation of the calcium-dependent protein kinase signaling pathway [18]. HDACs proteins, including HDAC5, play crucial roles in governing essential cellular processes, including cell cycle progression, differentiation, and tumorigenesis. Whether and how OGT regulates HDAC5 in the context of osteogenic differentiation and osteoporosis has not been reported.

In this study, we demonstrated OGT was down-regulated in PMOP, OGT is a regulator of osteoblastic differentiation, bone mass and bone loss following estrogen deficiency, OGT inhibition reduced osteogenic differentiation. OGT regulates osteogenesis by regulating HDAC5 and affecting histone acetylation modifications.

## 2. Materials and methods

### 2.1. Ethics statements

The Department of Orthopedics at the Second Affiliated Hospital of Chongqing Medical University gathered clinical samples in accordance with the applicable ethical guidelines (No. 2022302). The Animal Center of Chongqing Medical University approved all animal procedures and operations used in this study (No. CQLA-2022-0187).

### 2.2. Clinical samples

Human bone samples were obtained from vertebrae of 10 patients receiving Pedicle screw implantation. Before intraoperative pedicle screw implantation, a bone strip was taken from the vertebra through a biopsy puncture channel.

### 2.3. Mice

*Ogt*$^{fl/fl}$ and *Bglap*-Cre mice were purchased from the Cyagen Biosciences (No. CKOCMP-108155-Ogt-B6J-VA). To knockout *Ogt* in osteoblast, we cross-breeded *Ogt*$^{fl/fl}$ and *Bglap*-Cre mice. The mice were all C57BL/6 background mice, for all of the *Ogt* knockout investigations, we utilized littermate controls, *Ogt*$^{fl/fl}$ mice.

### 2.4. Cells

Mouse bone marrow mesenchymal stem cells (mBMSCs) were obtained from 2-week-old C57BL/6 mice as previously described [19], briefly, humeri, tibiae and femurs were digested with collagenase II for 30 min, and the digested bone fragments were cultivated in MEM Alpha Basic (Gibco) with 10 % fetal bovine serum (FBS), 100 mg/mL streptomycin and 100 units/mL penicillin, mBMSCs were used from passage 4 (P4). C3H10T1/2 and HEK293 cells were stored in our laboratory. C3H10T1/2 and HEK293 were cultured in DMEM with 10 % fetal bovine serum (FBS). For osteoblast (OB) differentiation, cells were switched to osteoblast differentiation medium, medium was changed every 3–5 days.

### 2.5. Cell proliferation and viability assay

Cell counting Kit-8 (Beyotime) was used to assess the cytotoxicity of OSMI-1 and (Z)-PUGNAc to cells in accordance with the manufacturer's instructions. Cells were cultured in 96-well plates, and various concentrations of OSMI-1 and (Z)-PUGNAc were then added and cultivated for 24, 48 h. Subsequently, the cells were treated at 37 °C with CCK-8 solution. Lastly, 450 nm was the wavelength used to measure absorbance.

### 2.6. Western blot analysis

Western blots were performed as described previously [20], briefly, Cells were scraped and lysed in RIPA-buffer with PMSF. Then, equal volumes of protein that had been denatured were separated using 10 % SDS-PAGE and then transferred to a PVDF membrane (Merck). After sealing the membrane with blocking buffer, it was left to incubate in the primary antibody solution for a whole night at 4 °C, including antibodies: beta-actin (Abclonal, AC026), HDAC5(Proteintech, 16166-1-AP), OGT (Proteintech, 11576-2-AP), O-GlcNAc (CST, 9875S), HA (Proteintech, 66006-2-Ig), Hey1 (Proteintech,19929-1-AP), Hey2 (Proteintech,10597-1-AP), HeyL(Abclonal, A17683). and then were developed after 1h incubation with the corresponding secondary antibody. Enhanced chemiluminescence (ECL; GE Healthcare) was used to detect protein bands, and ImageJ was used to quantify the protein.

### 2.7. Co-IP

Cells were lysed using IP lysis buffer (20 mM Tris–HCl, 150 mM NaCl, 1 mM EDTA,1 % Triton X-100) containing Protease and Phosphatase Inhibitor (Selleck). Protein A/G beads (Selleck) coated with primary antibodies were treated with cell lysates for 6 h at 4 °C, PBST rinsed three times, after which it was immunoblotted.

### 2.8. Quantitative real-time PCR

Following the directions provided by the manufacturer, total RNA was extracted from samples using an RNA-Quick Purification Kit (ES

Science). After reverse transcription, cDNA was mixed with 2x SYBR Green qPCR Master Mix (Selleck). qPCR was conducted using the Bio-Rad CFX apparatus. Table S1 contains a list of target gene primers.

### 2.9. Alkaline phosphatase and Alizarin red S staining

The cells were stained with alkaline phosphatase using the BCIP/NBT Alkaline Phosphatase Color Development Kit (Beyotime). As directed by the manufacturer, an Alkaline Phosphatase Assay Kit (Beyotime) was used to detect ALP activity. 405 nm was used to measure ALP activity (Thermo Varioskan LUX, USA).

The cells were washed and fixed with glutaraldehyde before being stained with Alizarin red S. The cells were then stained with 0.4 % ARS. ddH2O was used to wash the cells three times prior to taking pictures. Calcium nodules were dissolved in cetylpyridinium chloride monohydrate, and the optical density was measured at 540 nm (Thermo Varioskan LUX, USA).

### 2.10. Ovariectomy (OVX) mice

The operation was carried out under anesthetic, Ovariectomy was performed on eight-week-old female mice, Briefly, we performed two dorsolateral incisions to locate and exteriorize two ovaries in ovariectomy (OVX) group, and sham group underwent sham surgery. Upon removal of the ovaries, the peritoneal cavity and skin were closed. After 1 week or 8 weeks, the mice were administrated with DMSO or OSMI-1 (1 mg/kg) or (Z)-PUGNAc (10 mg/kg) by tail vein injection. The mice were given medication for eight weeks before being sacrificed for further research.

### 2.11. Histological staining

Samples of femurs were obtained, preserved in 4 % PFA, decalcified in 10 % EDTA, and then cut into sections that were 6 μm thick. Slides were stained with H&E and Trap staining. Immunohistochemistry was performed with an anti-OGT antibody (Proteintech, 11576-2-AP).

### 2.12. Micro–computed tomography (μCT) scanning

Mice femurs were scanned using a μCT system (Bruker SKYSCAN 1276). The following scanning parameters were set: 13 μm per slice at 100 μA of current and 60 kV of voltage. The interest region,150 slices from distal to proximal femur, was chosen for analysis. bone volume fraction (BV/TV), trabecular number (Tb. N.), trabecular thickness (Tb. Th.), and trabecular space (Tb. Sp.) were evaluated from 3D reconstruction images.

### 2.13. Three-point bending test

An electronic universal testing machine (GM-1000N) was used to assess the mechanical properties of femurs. The two supports were 8.0 mm apart, and load was applied at a constant speed of 5 mm/min to the femoral midshaft until fracture. The maximum bending loading and bending strength were recorded.

### 2.14. Immunofluorescence (IF)

After fixing cell slides with 4 % PFA, the specified primary antibody was left to incubate for an entire night. The cells were then stained with nuclear dye and mounted with DAPI after being treated with a secondary antibody tagged with fluorescence. A Leica confocal microscope (Leica TCS SP8) was used to capture the images.

### 2.15. Subcellular colocalization

Cells were seeded onto 20-mm glass bottom cell culture dish and transfected with plasmids, treated with (Z)-PUGNAc for 24 h before lysosome staining (50 nM LysoTracker Red; 60 min at 37 °C, Beyotime). Then, cells were stained with Hoechst (Beyotime). Last, A Leica confocal microscope (Leica TCS SP8) was used to capture the images.

### 2.16. RNA synthesis assay

Cells were glass seeded onto 15-mm coverslips, after 48 h of cultivation, cells were treated with 1 mM 5-EU (Beyotime) for 2 h, As directed by the manufacturer, the nascent RNAs were labelled with Alexa Fluor 594 (Beyotime), DNAs were labelled with Hoechst (Beyotime). A Leica confocal microscope (Leica TCS SP8) was used to capture the images.

### 2.17. Plasmid transfection

The full-length cDNA of mice HDAC5 (NM_001405237.1) was designed (ubigene, Guangzhou, China). The cDNA carried the green fluorescent protein (GFP) and HA Tag. HDAC5-T930A, HDAC5-T934A, HDAC5-S944A were constructed by overlapping PCR. DNA sequencing verified each creation. Plasmids were transfected using Lipo8000 (Beyotime).

### 2.18. siRNA

siRNA was transfected using Lipo8000(Beyotime). The sequences for OGT siRNAs were 5′-CUGCUUGGAUAAGAUUAAU-3′ (siOGT-1), 5′-GUGCACUGUUCAUGGAUUA-3′ (siOGT-2) and 5′-CUACGAGCAAGGCCUAAUA-3′(siOGT-3).

### 2.19. Analysis of single cell RNA sequencing

the human bone marrow mesenchymal stem cell scRNA-seq dataset was downloaded from the NCBI GEO database (GSE147287), and then use Seurat (version 4.0.5) to filtered barcode matrix files. For cells in a stress or apoptotic state, we filtered cells with >10 % mitochondrial gene content. To exclude empty droplets and potential cell diploidy, as well as cases where multiple cells were included in the same droplet, we filtered cells with gene numbers <200 or >8500. t-SNE was used for dimensionality reduction and then SPRING was used to visualize the data [21]. For DEGs, we used Wilcoxon test for analysis (log2 fc $\geq$ 0.25 and P-value<0.05). To simulate the cell differentiation process, we used Monocle2 to sort cells along their developmental trajectories based on differences in expression profiles of highly variable genes. and visualize the dynamic expression of OGT.

### 2.20. Identification of O-GlcNAcylated proteins

HPLC-MS/MS was performed to identify the O-GlcNAcylated proteins. In brief, as shown in Fig. 5A, cells were harvested on ice, and proteins were precipitated in acetone, reduction with TCEP, and then digested by trypsin, labelled with CH3CHO or $^{13}$CH3 [13]CHO, The labelled peptides were demineralized with C18 (Phenomenex, 15 μm, 300A), labelled-tryptic peptides were incubated with anti-O-GlcNAcylation antibody-conjugated protein A agarose beads at 4 °C overnight. Enriched peptides were reconstituted and then injected into Orbitrap Exploris 480 (Thermo Fisher Scientific), Dionex Ultimate 3000 RSLCnano (Thermo Fisher Scientific) for analysis. Scanning parameters were set as follows: Primary Mass spectrometry MS: The *m/z* range is 700~2000, the mass resolution is 60 k (*m/z* 200), the Automatic Gain Control Target (AGC Target) is $3 \times 10^6$, The Maximum Injection Time is 20 ms. Cascade Mass spectrometry MS/MS: Quality resolution 30k, Top 20 Data-Dependent Acquisition (DDA), automatic gain control target value $5 \times 10^5$, maximum ion implantation time 250 ms, the parent ion confinement Window (Isolation Window) is 1.4 *m/z*, the Dynamic Exclusion (Dynamic Exclusion) is 20.0 s, and the HCD stepped

collision normalized energy (stepped NCEs) is set at 30 %. The Uniprot database and O-GlcNAc database in Proteome Discoverer were used to create the search database. Set the number of missed cut sites allowed to 4 and select XCORR as the false discovery rate.

### 2.21. RNA-sequencing analysis

mBMSCs were isolated from the femur of *Ogt*$^{fl/fl}$ and *Ogt*$^{fl/fl}$; *Bglap*-Cre mice. Total RNA was extracted by using TRIzol reagent (Invitrogen, USA) following the manufacturer's instructions. Next, a Nano Drop and Agilent 2100 bioanalyzer (Thermo Fisher Scientific, MA, USA) were used to qualify and quantify total RNA, and the BGIseq500 sequencing platform was used for the sequencing process. Differentially expressed genes analysis was performed using DEseq2 (Fold Change$\geq$ 1.5 and Adjusted Pvalue $\leq$0.05). Phyper conducted GO and KEGG enrichment studies of DEGs based on the hypergeometric test in order to obtain insight into the change in phenotype.

### 2.22. Statistical analysis

Data are shown as mean ± SEM of at least three independent experiments by Student's t-test comparing two groups using unpaired two-tailed analysis with GraphPad Prism 9.5.0 (GraphPad Software Inc.).

## 3. Result

### 3.1. OGT is down-regulated in PMOP and up-regulated during osteogenic differentiation

First, we generated a gene set containing differentially expressed in postmenopausal women (PMW) and postmenopausal osteoporosis (PMOP) from NCBI data base (GSE35958). Compared to the group of postmenopausal women, we identified 852 differentially expressed genes (DEGs) ($P < 0.05$, |fold change|>1) (Fig. 1A and B), including key genes in osteoblasts such as LRP5(|logFC| = 1.78), OPN(|logFC| = 1.25), COL1A1 (|logFC| = 4.39) and SOST (|logFC| = 2.51). OGT attracted our attention due to our prior research on OGT [22], which is down-regulated in postmenopausal osteoporosis. To identify its level in vivo, we collected human vertebral cancellous bone, as determined by Western blot, the level of OGT and OGT-mediated O-GlcNAcylation decreased in postmenopausal osteoporosis (Fig. 1C– S1A). In addition, we created a mouse model of estrogen deficiency-induced bone loss using bilateral ovariectomy (OVX), in accordance with previous results, IHC results showed the level of OGT was decreased in ovariectomy (OVX) groups (Figs. S1B and C). To dynamically assess the level of OGT during the osteoblast to osteocyte maturation trajectory, we harnessed the power of single-cell RNA-seq (scRNA-seq). Through analysis of a recently reported scRNA-seq dataset obtained from femoral marrow of two human individuals' mesenchymal stem cells [23], Based on previous reports [24–26], the different types of cells were annotated as: MSC (LEPR$^{+}$; CD45$^{-}$); Osteoblast precursor (Collagen1$^{+}$; ALPL$^{+}$); Adipocyte precursor (Adipoq$^{+}$; MGP$^{+}$); Chondrocyte precursor (CD56$^{+}$; Wif1$^{+}$), we captured seven distinct bone lineage clusters and reconstructed developmental trajectory by inferring dynamic gene expression patterns at different stages of development, suggesting that bone marrow mesenchymal stem cells have multi-lineage differentiation potential (Fig. 1D–G). The dynamic gene expression pattern of OGT showed that OGT increased over time during osteogenesis (Fig. 1H). To the end, the levels of OGT and O-GlcNAcylation increased in mBMSCs during osteogenic differentiation, as measured by western blot (Fig. 1I–J). These results suggest that OGT plays a critical role in osteogenic differentiation.

### 3.2. OGT-mediated O-GlcNAcylation protects mice from ovariectomy (OVX)-induced bone loss

To investigate the physiological role of OGT-mediated O-GlcNAcylation in vivo. We established an estrogen-deficient bone-loss model by using bilateral ovariectomy (OVX), and OSMI-1 (1 mg/kg) or (Z)-PUGNAc (10 mg/kg) was administered via tail vein (Fig. 2A). OSMI-1 is a kind of cell-permeable O-GlcNAc transferase (OGT) inhibitor which repressed the occurrence of O-glycosylation [27], on the other hand, (Z)-PUGNAc serves as a potent inhibitor of O-GlcNAcase, increasing O-GlcNAcylation by blocking the glycoside hydrolase O-GlcNAcase (OGA) [27]. Inhibiting OGA reduces the level of O-GlcNAcylation and inhibiting OGT increases the level of O-GlcNAcylation (Fig. S2B). MicroCT (μCT) scanning of the femur revealed bone volume/total volume (BV/TV), trabecular thickness (Tb.Th.), trabecular number (Tb.N.) in ovariectomy (OVX) mice were significantly decreased and trabecular separation (Tb.sp) was significantly increased, as compared with sham mice. Interestingly, the change in bone mass was partially restored following treatment with (Z)-PUGNAc (Fig. 2B, E-H). However, there was no notable alteration in bone mass in the OSMI-1 group, which we hypothesized was due to the relatively low OGT level in ovariectomy (OVX) model mouse (Fig. S1B), so the effect of inhibiting OGT was limited. H&E staining of femur was used to further evaluate the bone tissue microstructure. Compared with ovariectomy (OVX) mice, the osteoporotic phenotype of (Z)-PUGNAc-treated ovariectomy (OVX) mice was significantly improved, as confirmed by quantitative histomorphometric analysis of BS (Fig. 2C–I). TRAP staining was used to exclude that the observed effects on bone mass were mediated by osteoclasts, and showed the number of osteoclasts increased in the ovariectomy (OVX) model group, but no difference in the ovariectomy (OVX) group treated with inhibitors or not (Fig. 2D, J). In addition, we go through another mode of administration——8 weeks after ovariectomy (OVX), consistent with the previous results, Micro-CT showed that femoral bone mass in ovariectomy (OVX) mice was significantly reduced, and bone mass partially recovered after treatment with (Z)-PUGNAc (Fig. S2A, C-F). These results demonstrated that OGT-mediated O-GlcNAcylation plays a role in bone formation following estrogen deficiency.

### 3.3. Ogt conditional knockout (cKO) mice exhibit lower bone mass

To further investigate the physiological role of OGT in bone, we generated *Ogt* cKO mice (Fig. 3A). We conditionally deleted *Ogt* by crossing *Ogt*$^{fl/fl}$ mice with *Bglap*-Cre mice to knockout *Ogt* in *Bglap*-expressing cells, Genotyping and detection of *Ogt* expression verified the knockout of *Ogt* in bone tissue (Fig. 3B, S3A, B). Compared to *Ogt*$^{fl/fl}$ littermate controls, *Ogt*$^{fl/fl}$; *Bglap*-Cre (*Ogt* cKO) mice showed a significant decrease in weight after 5 weeks of age and a smaller size at 12 weeks of age (Fig. 3C, S3C). Micro CT (μCT) scanning of *Ogt*$^{fl/fl}$ control and *Ogt* cKO mice showed bone volume/total volume (BV/TV), trabecular thickness (Tb.Th.), trabecular number (Tb.N.) in *Ogt*$^{fl/fl}$; *Bglap*-Cre mice were significantly decreased and trabecular separation (Tb.sp) was significantly increased, as compared with those of *Ogt*$^{fl/fl}$ mice. Intriguingly, the degree of bone loss is more severe in male mice compared to female mice (Fig. 3D and E). This may be associated with the.

*Ogt* gene located on the X chromosome. The decrease in bone mass in *Ogt*$^{fl/fl}$; *Bglap*-Cre mice, was associated with descending bone mechanical strength, as measured by three-point bending test (Fig. 3F and G). H&E and Masson's trichrome staining of femur was used to further evaluate the bone tissue microstructure. Consistent with the previous results, *Ogt*$^{fl/fl}$; *Bglap*-Cre mice showed a reduced bone volume (Fig. 3H). Meanwhile, we isolated BMSCs from *Ogt*$^{fl/fl}$ and *Ogt*$^{fl/fl}$; *Bglap*-Cre mice and induced them into osteoblast respectively, it is showed that ALP staining intensity, ALP activity and mineralized matrix formation were reduced in the *Ogt*-deficient BMSCs (Fig. 3I–L). These results

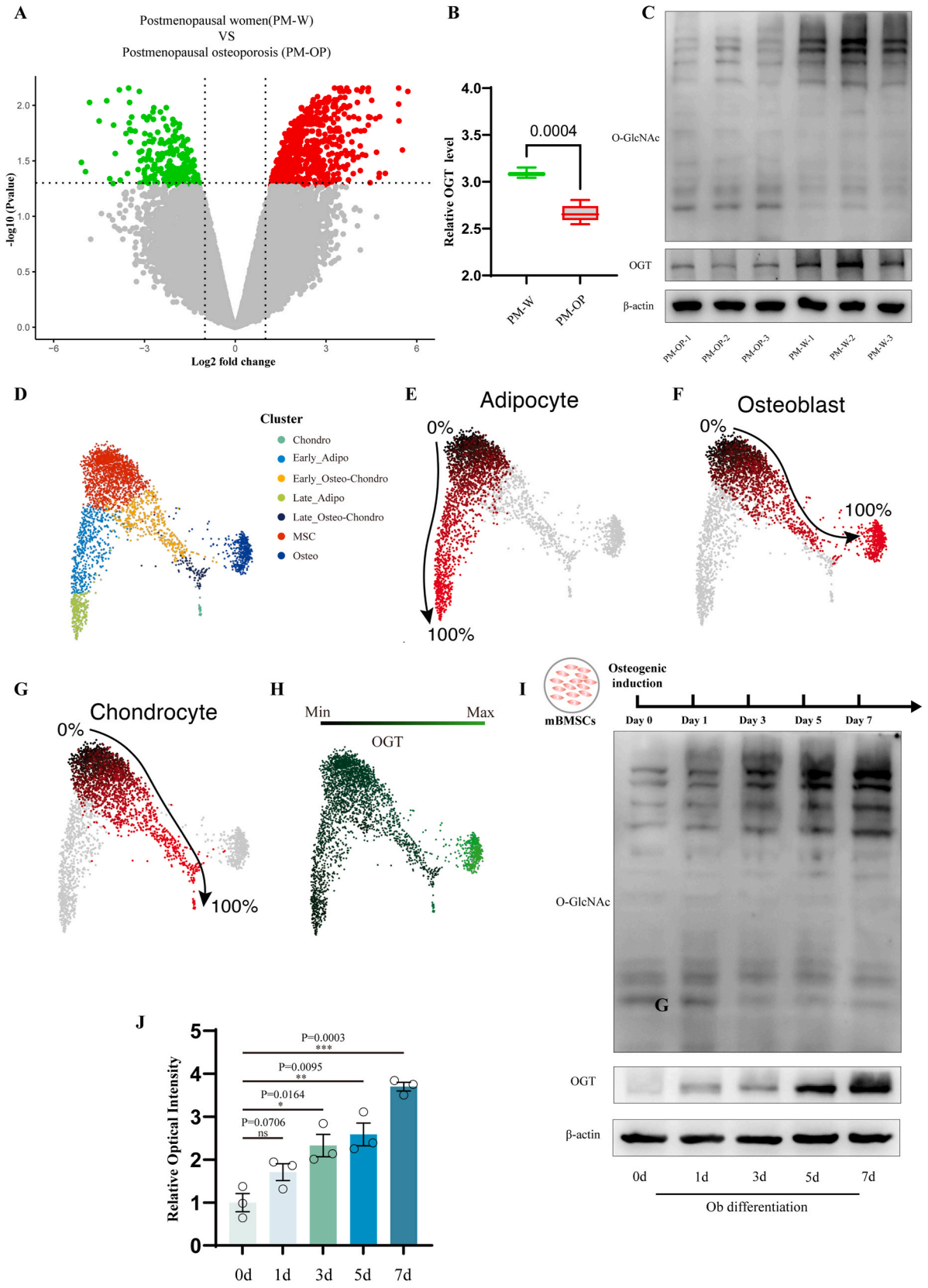


**Figure 1.** OGT is down-regulated in PMOP and up-regulated during osteogenic differentiation. **(A)** A volcano plot of mRNAs between postmenopausal women (PM-W) and postmenopausal osteoporosis (PM-OP). **(B)** *Ogt* was downregulated in postmenopausal osteoporosis. **(C)** Western blot assays showed the level of OGT and O-GlcNAcylation in PM-W and PM-OP (n = 3). **(D)** t-SNE visualization of human mesenchymal stem cells. **(E–G)** Pseudotemporal annotation of the human mesenchymal stem cells developmental tree. **(H)** Expression of *Ogt* in each cell plotted against the cell's position in pseudotime. **(I–J)** Western blot assays showed the level of OGT and O-GlcNAcylation during osteogenic differentiation. Data are represented as mean ± SEM. P-values are shown in the graphs.

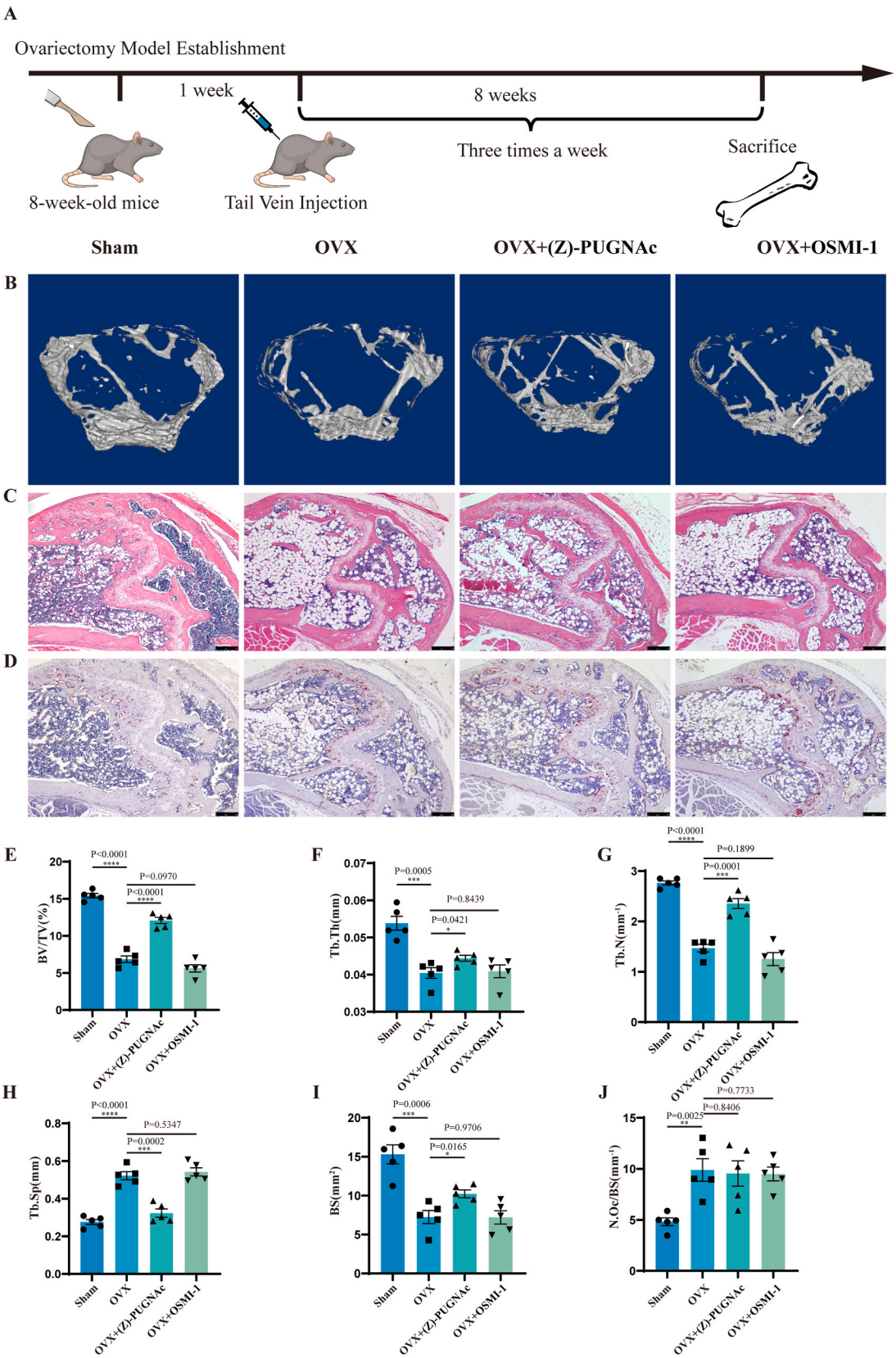


**Figure 2.** OGT-mediated O-GlcNAcylation protects mice from ovariectomy(OVX)-induced bone loss. **(A)** Schematic diagram representing the medication strategy (n = 5). **(B)** Representative 3D micro-CT reconstruction images(n = 5) (scale bars = 250 μm). **(C)** Representative H&E staining images of femur (scale bars = 250 μm). **(D)** Representative TRAP staining images of femur (scale bars = 250 μm). **(E–H)** Quantitative analysis of bone parameters. (E) BV/TV (%). (F) Tb.Th (mm). (G) Tb.N ($mm^{-1}$). (H) Tb.sp (mm). **(I)** Quantitative analysis of histomorphometric bone parameters of BS (mm2). **(J)** Number of $TRAP^{+}$ cells on the trabecular bone surface (N.Oc/BS, $mm^{-1}$). Data are represented as mean ± SEM. P-values are shown in the graphs.

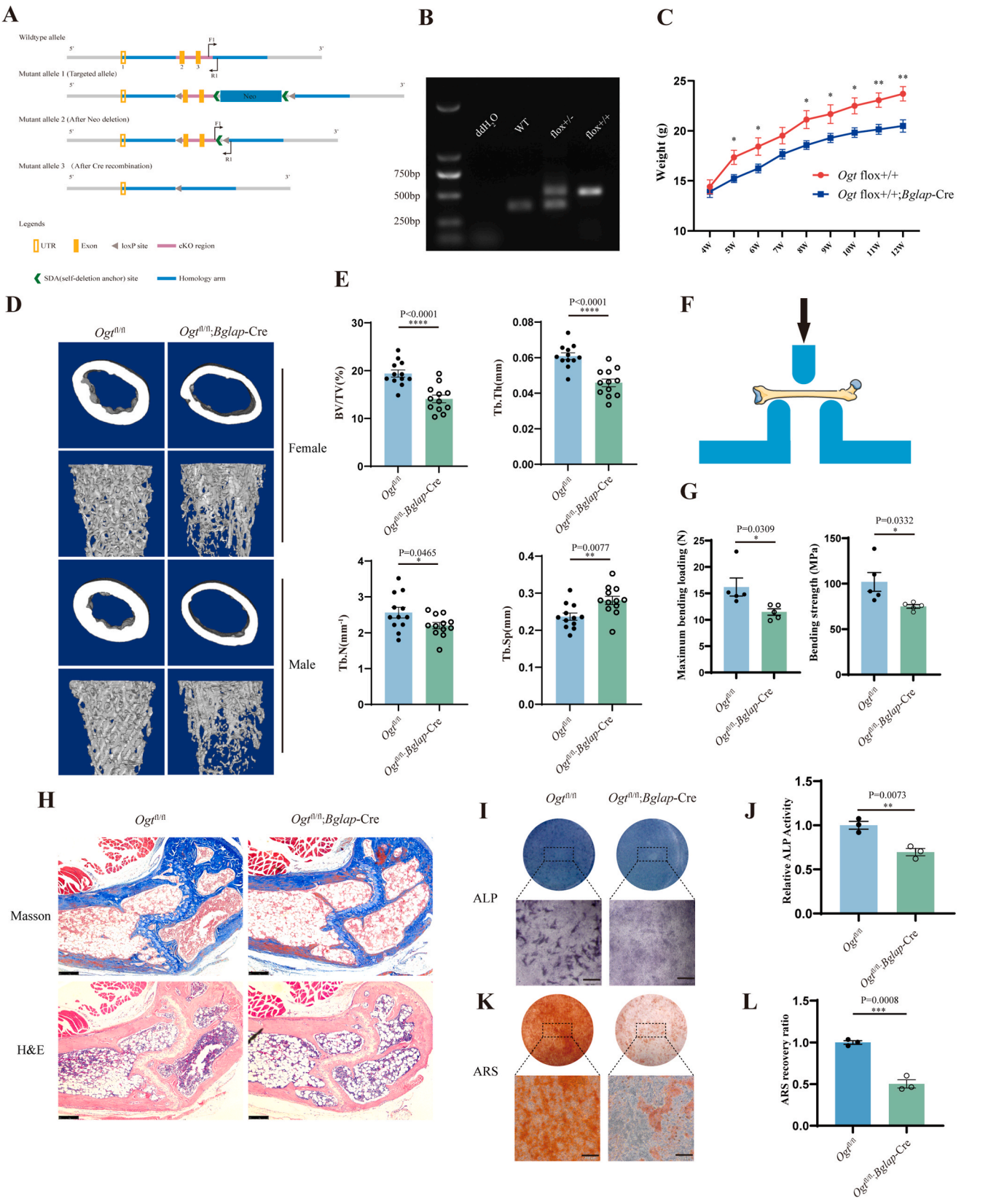


**Figure 3.** *Ogt* conditional knockout (cKO) mice exhibit lower bone mass. **(A)** Schematic diagram showing the strategy for *Ogt* deletion. **(B)** DNA electrophoresis was performed to genotype genetically modified mice (Homozygotes = 502bp, Wildtype = 377 bp). **(C)** Body weights of $Ogt^{fl/fl}$ and $Ogt^{fl/fl}$; *Bglap*-Cre mice. **(D)** Representative 3D micro-CT reconstruction images(n = 12). **(E)** Quantitative analysis of bone parameters. BV/TV (%), Tb.Th (mm), Tb.N ($mm^{-1}$), Tb.sp (mm). **(F, G)** Three-point bending test was measured on femur of $Ogt^{fl/fl}$ and $Ogt^{fl/fl}$; *Bglap*-Cre mice and quantitated by maximum bending loading (N) and bending strength (MPa) (n = 5). **(H)** Representative H&E and Masson's trichrome staining images of femur (scale bars = 250 μm). **(I–L)** Alkaline phosphatase (ALP) activity, ALP staining and Alizarin Red staining of mBMSC (scale bars = 200 μm). Data are represented as mean ± SEM. P-values are shown in the graphs.

demonstrated that OGT was involved in bone formation and OGT plays a vital role in osteogenesis.

### 3.4. OGT-mediated O-GlcNAcylation promotes osteogenic differentiation of mBMSCs

To ascertain the function of OGT-mediated O-GlcNAcylation in osteogenic differentiation in vitro, we treated mBMSCs during osteogenic differentiation with OSMI-1, a widely used specific inhibitor of OGT [27], to decrease the O-GlcNAcylation level, or (Z)-PUGNAc, a specific inhibitor of OGA [28], to increase the O-GlcNAcylation level. Firstly, OGT inhibition (10 μM) or OGA inhibition (20 μM) did not impair the proliferation of mBMSCs (Fig. 4A and B). Then inhibition of OGA enhanced osteogenic differentiation evidenced by higher levels of RUNX2, ALP, OPN, COL1A1, higher ALP staining intensity, higher ALP activity and higher mineralized matrix formation. On the other hand, inhibition of OGT leads to the reduction of osteogenic differentiation (Fig. 4C–L). Those findings were further confirmed by siOGT or overexpressing OGT in C3H10T1/2 (Figs. S4A–H). The results further demonstrated that OGT was a positive regulator for osteogenic differentiation in vitro.

### 3.5. Identification of the substrates of OGT-mediated O-GlcNAcylation

To understand the endogenous O-GlcNAcylation substrates mediated by OGT, as shown in Fig. 5A, we performed quantitative proteomics by combining affinity enrichment and isotope tag to clarify the effects of O-GlcNAcylation on substrates. A total of 1534 unique O-GlcNAcylated sites, 1527 unique O-GlcNAcylated peptides, and 924 O-GlcNAcylated proteins were identified (Fig. 5B). Normalizing the detected abundances to the expression of their corresponding proteins, we quantified 374 significantly downregulated and 55 significantly upregulated proteins (more than 2x) (Fig. 5C). To understand the biological significance of OGT-mediated O-GlcNAcylation, we further performed KEGG and Gene Ontology (GO) analysis, KEGG analysis showed that OGT was significantly enriched in multiple signaling pathways related to osteogenic differentiation, such as: Hedgehog signaling pathway [29], Hippo signaling pathway [30], VEGF signaling pathway [31], Notch signaling pathway [32], among others (Fig. 5D). The GO analysis revealed significant enrichment of these signaling pathways in processes related to osteogenic differentiation, collagen trimer formation, extracellular matrix, and other associated activities (Fig. 5E). To identify key proteins involved in O-GlcNAcylation, the protein–protein interaction (PPI) networks were constructed and presented that O-GlcNAcylated proteins might be involved in regulatory osteogenic differentiation through HDAC5, Hey1 and HeyL, which are components of the Notch signaling pathway and connected with bone development [33] (Fig. 5F). To further explore the mechanism of OGT-mediated O-GlcNAcylation on osteogenic differentiation, transcriptome high-throughput RNA sequencing (RNA-seq) assay were performed in control and *Ogt*-deficient BMSCs. Totally, we identified 702 significantly downregulated and 228 significantly upregulated differentially expressed genes (DEGs) (Figs. S5A and B). KEGG and GO analysis revealed a significant enrichment of categories pertinent to osteogenic differentiation for OGT (Figs. S5C and D). Gene set enrichment analysis (GSEA) showed that *Ogt* deletion was closely associated with downregulation of O-Glycosylation, extracellular matrix structural constituent, and osteoblast differentiation ($P < 0.05$) (Figs. S5E–G). Comparing quantitative proteomics and RNA-seq datasets, a total of 32 overlapping proteins(genes), including Col1a1, Hdac5, Ildr2, were observed (Fig. S5H).

### 3.6. O-GlcNAcylation of HDAC5 promotes its proteolysis by autophagy-lysosomal pathway

As high-throughput data analysis presented, HDAC5 was an important overlapping protein(gene) in quantitative proteomics and RNA-seq datasets. It is reported that HDAC5, a histone deacetylase enzyme, plays a crucial role in influencing epithelial differentiation and morphogenesis through the activation of genes targeted by MEF2 during the transcription process [34,35]. To confirm the O-GlcNAcylation of HDAC5, co-immunoprecipitation (Co-IP) assay was performed to demonstrate the interaction between OGT and HDAC5 in mBMSCs (Fig. 6A), and the co-IP assay revealed HDAC5 displayed a distinct O-GlcNAcylation signal in mBMSCs that were treated with OSMI-1 or (Z)-PUGNAc (Fig. 6B). Next, to investigate the effect of O-GlcNAcylation on HDAC5, we first examined the mRNA level of HDAC5 in mBMSCs after treatment with different dose of OGT inhibitor or OGA inhibitor and found that, compared to the DMSO, (Z)-PUGNAc treatment increased the mRNA levels of HDAC5, and OSMI-1 decreased (Fig. 6C and D). We then detected the protein level of HDAC5, and found that, (Z)-PUGNAc treatment reduced the amount of HDAC5, whereas OSMI-1 increased it (Fig. 6E–H), and it is also consistent with the immunofluorescence data (Fig. 6I and J). Under the same treatment conditions, with mRNA levels and protein levels exhibiting completely opposite trends, it was suggested that HDAC5 may undergo post-translational modifications followed by subsequent degradation. Since protein degradation occurs through proteasomal, endosomal, and lysosomal pathways [36], Proteasome inhibitor MG132 and autophagy inhibitor bafilomycin A1 (BafA1) were used to determine the pathway by which (Z)-PUGNAc facilitates OGT-mediated O-GlcNAcylation of HDAC5, ultimately leading to its degradation. The data indicated that BafA1 effectively prevented the reduction of HDAC5 caused by (Z)-PUGNAc in mBMSCs. In contrast, MG132 did not exhibit the same inhibitory effect (Fig. 6K–N). Overall, these results indicated that O-GlcNAcylation of HDAC5 induces its degradation through autophagy-lysosomal system.

### 3.7. HDAC5 inhibitor partially reversed bone mass loss in Ogt cKO mice

We detected the protein level of HDAC5 in bone tissue of $Ogt^{fl/fl}$ and $Ogt^{fl/fl}$; *Bglap*-Cre mice, and in agreement with the previous results, $Ogt^{fl/fl}$; *Bglap*-Cre mice exhibited higher HDAC5 levels (Figs. S6A and B). In order to further confirm the role of HDAC5 in *Ogt* cKO mice, *Ogt* cKO mice were injected with BRD4354, an HDAC5 inhibitor, twice a week via tail vein (Fig. S6C). BRD4354 treatment reduced bone loss in *Ogt* cKO mice compared to DMSO control group, as evidenced by micro CT (μCT) (Fig. S6D). Micro CT (μCT) scanning of the femur revealed that bone volume/total volume (BV/TV) and trabecular thickness (Tb.Th.) were significantly increased in the *Ogt* cKO mice treated with BRD4354 compared to DMSO group (Figs. S6E–H). Furthermore, BRD4354 treatment improved bone mechanical strength of *Ogt* cKO mice compared with that of control, as measured by 3-point bending test, both maximum bending loading and bending strength were significantly increased (Figs. S6I–K).

### 3.8. Thr934 is the O-GlcNAcylation site of HDAC5

To identify the O-GlcNAcylation site(s) on HDAC5, we reanalyzed the mass spectrometry data and found that Thr934 (T934) was the primary O-GlcNAcylation site on HDAC5(Fig. 7A), interestingly, HDAC5 T934 exhibits strong preservation across a wide range of species (Fig. 7B). Strikingly, when T934 was mutated to alanine, the O-GlcNAc signal exhibited a significant reduction compared to the HDAC5-WT, T930A or S944A mutants in HEK293 cells (Fig. 7C). Furthermore, HA-tagged HDAC5-WT or HDAC5-T934A were overexpressed in C3H10T1/2, after T934 was mutated, its O-GlcNAc signal was no longer affected by (Z)-PUGNAc (Fig. 7D). To visualize the effect of T934 O-GlcNAcylation on HDAC5 directly, we co-localized GFP-HDAC5 with LysoTracker——an indicator of lysosomes, the HDAC5-T934 mutant proteins were no longer transported to lysosomes, compared to wild-type HDAC5 (Fig. 7E), suggesting that T934 was the major O-GlcNAcylation site of HDAC5. Since HDAC5, a member of Class IIa HDACs, plays an important role in regulating gene expression, the nascent RNA

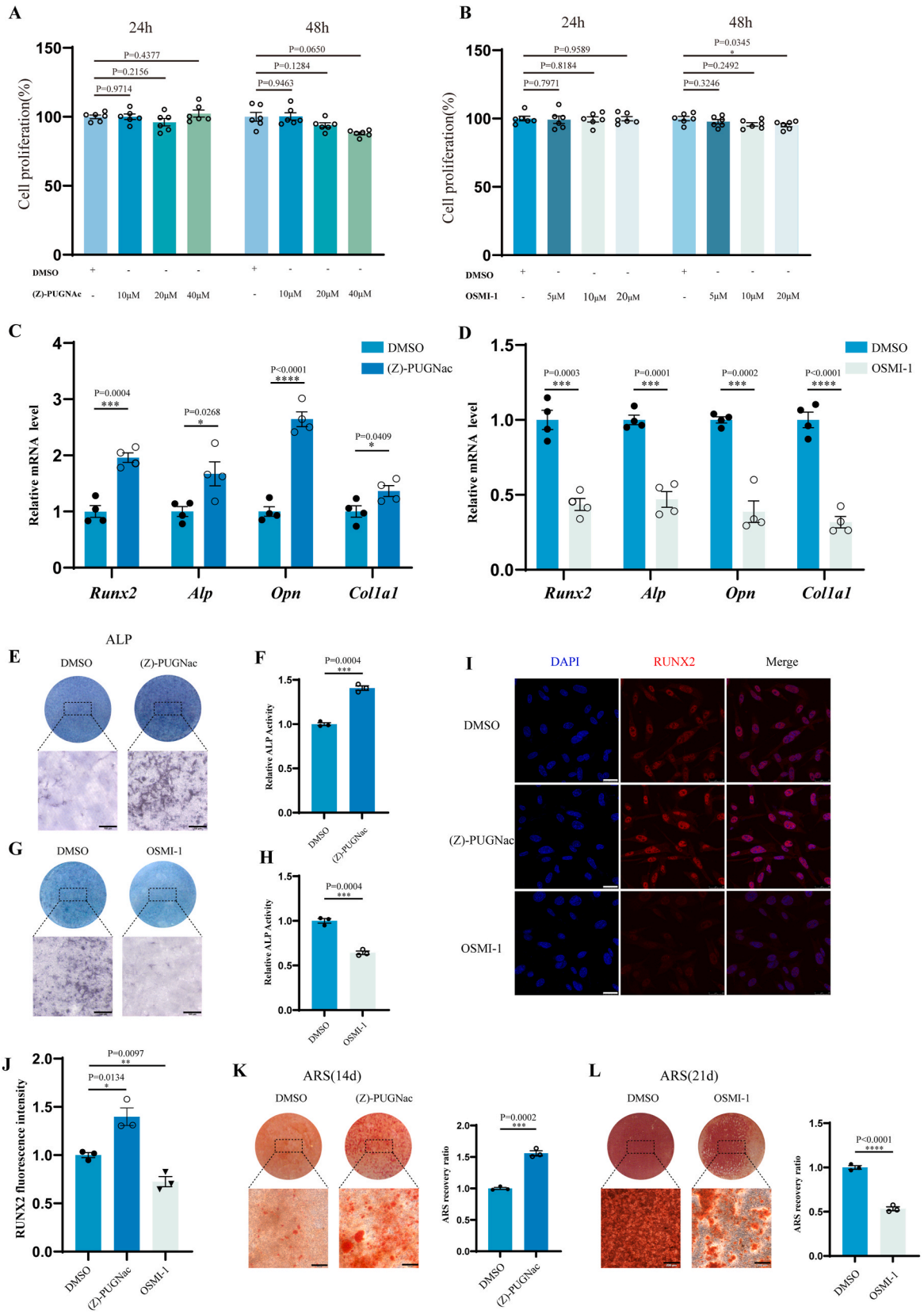


**Figure 4.** OGT-mediated O-GlcNAcylation promotes osteogenic differentiation of mBMSCs. **(A, B)** Proliferation assay of mBMSC treated with OSMI-1 or (Z)-PUGNAc. **(C, D)** mRNA levels of osteogenesis-related genes of mBMSC treated with OSMI-1 or (Z)-PUGNAc. **(E–H)** Alkaline phosphatase (ALP) activity and ALP staining of mBMSC treated with OSMI-1 or (Z)-PUGNAc (scale bars = 100 μm). **(I, J)** Immunofluorescence microscopy with antibodies against RUNX2 of mBMSC treated with OSMI-1 or (Z)-PUGNAc(n = 3) (scale bars = 25 μm). **(K, L)** Alizarin Red staining of mBMSC treated with OSMI-1 or (Z)-PUGNAc (scale bars = 100 μm). Data are represented as mean ± SEM. P-values are shown in the graphs.

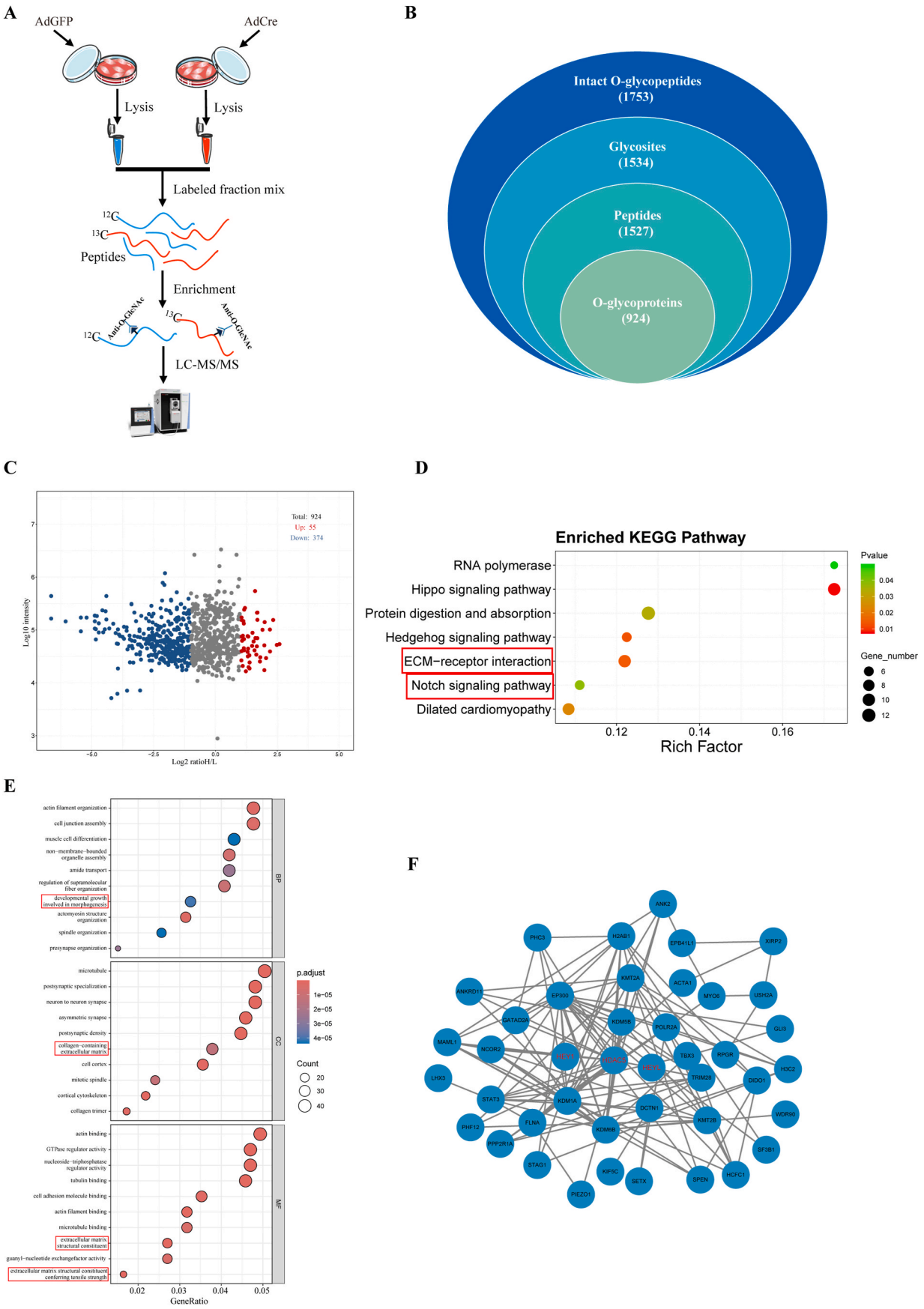


**Figure 5.** Identification of the substrates of OGT-mediated O-GlcNAcylation. **(A)** Schematic diagram showing workflow of quantitative O-GlcNAcylation proteomic analysis. **(B)** Venn diagram of O-GlcNAcylation proteomic analysis. **(C)** Scatterplot showing the intensity ratio of O-GlcNAcylation peptides. **(D, E)** KEGG analysis and GO analysis for O-GlcNAcylation proteins. **(F)** Protein–protein interaction (PPI) networks showing the interaction of O-GlcNAcylated proteins.

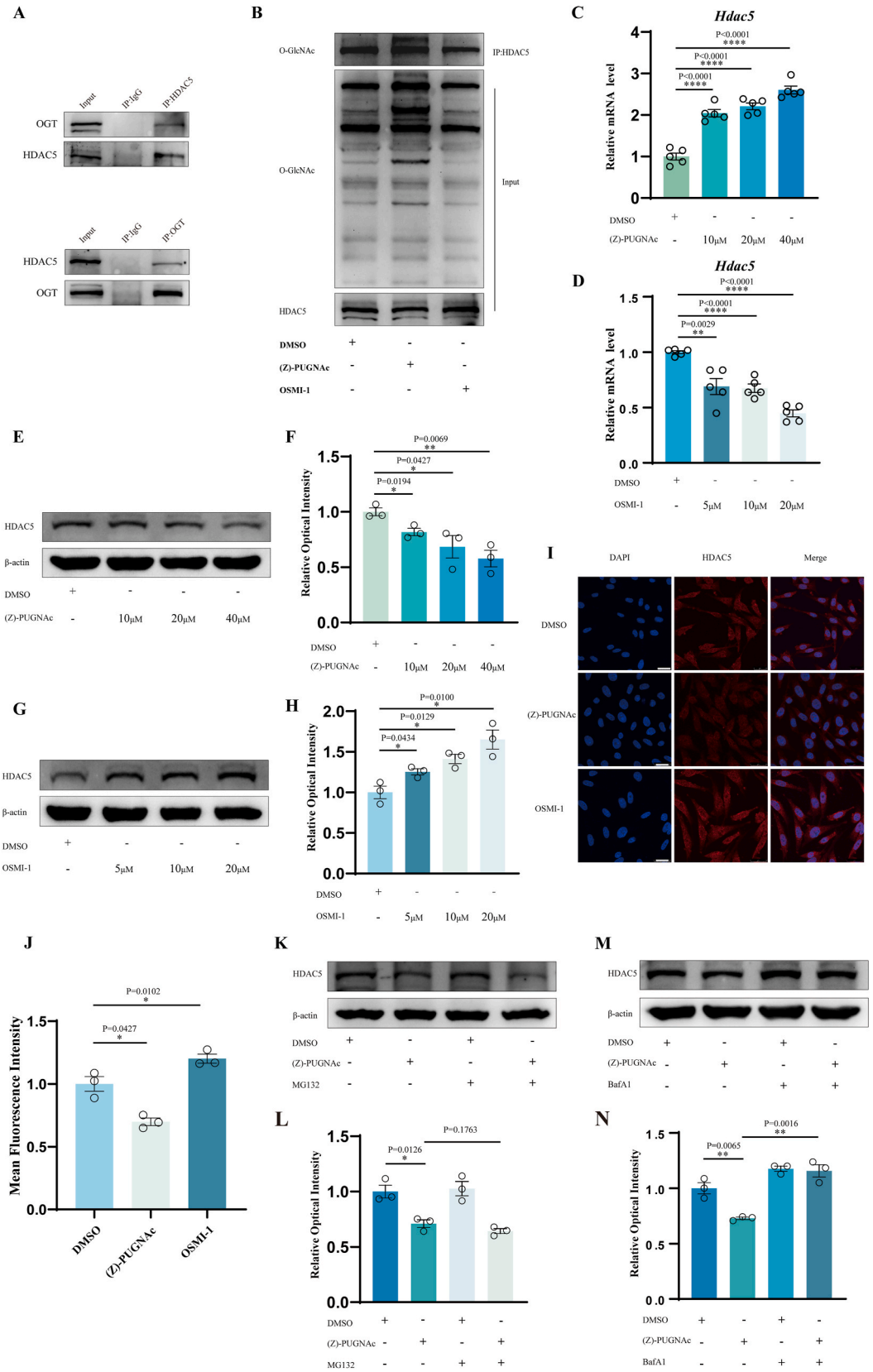


**Figure 6.** O-GlcNAcylation of HDAC5 promotes its proteolysis. **(A)** Co-IP of endogenous OGT and HDAC5 in mBMSC. **(B)** Levels of O-GlcNAcylation on HDAC5 in mBMSC treated with OSMI-1 or (Z)-PUGNAc by immunoprecipitation. **(C–D)** HDAC5 mRNA levels in mBMSC treated with OSMI-1 or (Z)-PUGNAc. **(E–H)** HDAC5 proteins levels in mBMSC treated with OSMI-1 or (Z)-PUGNAc. **(I, J)** Immunofluorescence microscopy with antibodies against HDAC5 of mBMSC treated with OSMI-1 or (Z)-PUGNAc(n = 3) (scale bars = 25 μm). **(K, L)** mBMSC were treated with 10 μM MG132 for 6h before harvest. **(M, N)** mBMSC were treated with 100 nM bafilomycin A1 (BafA1) for 6h before harvest. Data are represented as mean ± SEM. P-values are shown in the graphs.

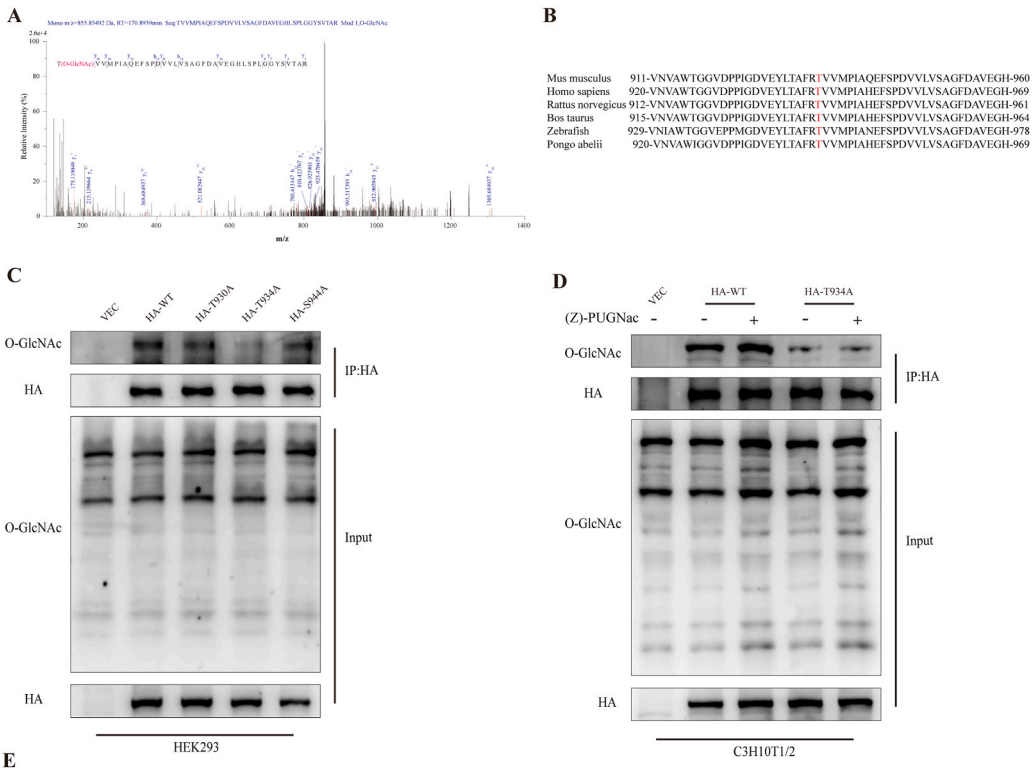


*(caption on next page)*

**Figure 7.** Thr934 is the major O-GlcNAcylation site of HDAC5. **(A)** LC-MS analysis identified residue Thr934 as the HDAC5 O-GlcNAcylation site. **(B)** Cross-species sequence alignment of HDAC5. **(C)** Immunoprecipitation with anti-HA in HEK293 cells. Cells were transfected with vectors encoding HA-tagged HDAC5 (WT, T930A, T934A or S944A). **(D)** C3H10T1/2 cells (with or without (Z)-PUGNAc) were transfected with HA-tagged HDAC5 (WT or T934A), and subjected to immunoprecipitation (VEC=Vector). **(E)** Colocalization of HDAC5 and LysoTracker in C3H10T1/2 cells. Cells were transfected with vectors encoding GFP-HDAC5 (WT or T934A) (scale bars = 10 μm), White arrows show lysosomes. **(F, G)** Fluorescence microscopy with nascent RNA in C3H10T1/2 cells (scale bars = 50 μm). Data are represented as mean ± SEM. P-values are shown in the graphs.

was labelled by 5-ethynyluridine (EU) to identify the effect of HDAC5 on the transcription of the DNA. The EU-labelled nascent RNA is detected by using click chemistry with fluorescent azides, Fluorescence imaging revealed HDAC5 could inhibit the transcription (Fig. 7F and G). Next, we also examined the effect of OGT on gene transcription during osteogenic differentiation, we treated BMSCs with 10 μM OSMI-1, fluorescence imaging revealed OSMI-1 could inhibit the gene transcription during inhibition of the O-glycosylation, which was also confirmed in the *Ogt*-deficient BMSCs (Fig. 8A and B). As Fig. 5 exhibited by the affinity enrichment results of O-GlcNAcylation on substrates in quantitative proteomics, OGT is closely associated with some signaling pathways related to osteogenic differentiation, including Notch signaling, consistent with literature reports [37,38]. We then examined the expression of Notch effector molecules——Hey1, Hey2, and HeyL. The protein levels of Hey1, Hey2, and HeyL were downregulated in *Ogt*-deficient BMSCs (Fig. 8C and D). and we also examined the expression of Hey1, Hey2, and HeyL in C3H10T1/2 cells transfected with vectors, HDAC5-WT or HDAC5-T930A, the mRNA levels of Hey1, Hey2, and HeyL were downregulated in cells transfected with HDAC5-WT or HDAC5-T930A (Fig. 8E). To achieve the purpose of treating osteoporosis, A small bioactive molecule silymarin extracted from *Silybum marianum* was identified as the OGT agonist using a traditional Chinese medicine database search and molecular docking showed that and silymarin binds to the OGT protein with a binding energy of $-7.463$ kcal $mol^{-1}$(Fig. 8F), and subsequent experiments confirmed that that silymarin can increase the protein level of OGT (Fig. 8G).

## 4. Discussion

Bone homeostasis depends on osteoclast-induced bone resorption and osteoblast-induced bone reconstruction, BMSC, as a major source of osteoblasts, is essential in maintaining bone homeostasis, and reduced osteogenic differentiation capacity can lead to osteoporosis and other orthopedic diseases [39]. Using analyses of RNA-seq and scRNA-seq, we identified OGT as a pivotal OP-related gene in MSC osteogenesis [23,40], and substantiated that OGT was essential for MSC osteogenesis in vitro and in vivo, as well as for OP, revealing the crucial role of protein O-GlcNAcylation in osteogenic differentiation.

We observed lower level of OGT in postmenopausal women with osteoporosis compared to postmenopausal women without osteoporosis. OGT, catalyzes the transfer of GlcNAc moiety onto the serine (S) or threonine (T), is responsible for the O-GlcNAcylation of proteins. O-GlcNAcylation is the modification of proteins by carbohydrates [41]. It is one of the most abundant PTMs in all cells and related to transcriptional regulation, calcium signaling and cell survival etc [42]. O-GlcNAcylation has been implicated in the pathogenesis of various human diseases [43–48], however, O-GlcNAcylation in bone development and remodeling has been poorly studied. In this study, we pharmacologically inhibited OGT by OSMI-1 or OGA by (Z)-PUGNAc to block or promote the process of O-GlcNAcylation in ovariectomy (OVX) mice. (Z)-PUGNAc targeting OGA increases O-GlcNAcylation levels, which can promote osteoblast differentiation and ameliorate ovariectomy (OVX)-induced bone loss. TRAP staining showed that osteoclasts in the ovariectomy (OVX) group were not significantly altered by OSMI-1 or (Z)-PUGNAc, excluded that the observed effects on bone mass in ovariectomy (OVX) mice were related to osteoclastogenesis. Since, it has been reported that O-GlcNAcylation could regulate osteoclast differentiation [49–51],those studies focused on the role of O-GlcNAcylation in inflammation-induced osteoclastogenesis. A recent study has shown that O-GlcNAcylation may have an impact on inflammation [52], so the regulation on inflammation induced osteoclastogenesis may mediate by modulation of inflammation, and osteoclast differentiation requires dynamic regulation, both OGT and OGA inhibitor inhibit osteoclastogenesis [50,53]. Herein, we observed the decreased bone intensity in the *Ogt* $^{fl/fl}$; *Bglap*-Cre mice with deletion of *Ogt* in osteoblasts, and the results observed in ovariectomy (OVX) mice cannot be fully explained by the potential effects on osteoclasts but are rather attributed to the impact on osteoblasts. A recent study demonstrated the same results in $Ogt^{fl/fl}$; *Sp7*-Cre mice with cKO of *Ogt* in bone mesenchymal stem/progenitor cells [16]. These results indicated that MSC osteogenesis exhibits constantly increasing levels of O-GlcNAcylation and OGT plays an important role in different stages of MSC osteogenesis.

Mechanistically, Quantitative proteomics and RNA-seq showed HDAC5 is a substrate of OGT-mediated O-GlcNAcylation. Indeed, HDAC5 is a newly identified OGT-targeted O-GlcNAcylation substrate, with Thr934 (T934) being the primary O-GlcNAcylation site on HDAC5. Once the T934A is mutated, HDAC5 cannot undergo O-GlcNAcylation modifications. It is known that O-GlcNAcylation more commonly stabilizes protein substrates by antagonizing ubiquitination [54,55]. Interestingly, our study found that O-GlcNAcylation of HDAC5 promotes its lysosomal degradation, resulting in inconsistent mRNA and protein changes, recently some studies have also reported the destabilizing effect of O-GlcNAcylation in receptor-interacting protein kinase 3 (RIPK3), forkhead box protein A2 (FoxA2), Hepatocyte Growth Fctor-Regulated Tyrosine Kinase Substrate (HGS) [56–58]. These findings indicate a diverse role for O-GlcNAcylation in the regulation of protein substrates.

HDAC5, a part of Class IIa HDACs, is responsible for removing acetyl group from the histones comprising the nucleosome leading to histone hypoacetylation, then leads to transcription inactivition. In this way, Histones can alter the way DNA wraps around them, affecting the folding conditions of promoter regions and inhibiting gene expression [59]. Literature suggests that inhibitors of HDACs may extend human lifespan [60], HDACs inhibitors can provide prophylactic treatment for many disease, such as: neurodegeneration [61], cardio-metabolic diseases [62], arthritis [63] and premature aging [64]. Previous genome-wide association analysis showed that only HDAC5 in the HDACs family is associated with human bone mass [65]. And previous study has shown that HDAC5 accumulation leads to degradation of Runx2 and inhibition of HDAC5 can increase Runx2 acetylation and ultimately enhance osteoblast differentiation [66]. In our study, we demonstrated that a HDAC5 inhibitor——BRD4354 can partially reverse bone mass loss in *Ogt* cKO mice, which indicates repressing the function of HDAC5 can improve the osteogenic differentiation of MSCs. Thus, our findings unveil a novel interplay between O-GlcNAcylation and acetylation, introducing a unique regulatory mechanism for HDAC5. Additionally, we demonstrate, for the first time, the indispensable role of OGT-HDAC5 signaling in osteogenic differentiation. As literature reported, Hey1, Hey2 and HeyL are the best known Notch effector molecules in mammals. HDAC5 can directly inhibit the expression of Hey1, Hey2 and HeyL [37]. Herein, the expression of Hey1, Hey2, and HeyL is reduced in *Ogt* cKO mBMSCs. Of note, studies have shown that the reduction of Hey gene expression directly inhibits osteogenic differentiation and promotes osteoclast generation, thus leading to osteogenic defects [67,68].

In summary, we found that OGT constantly increases during

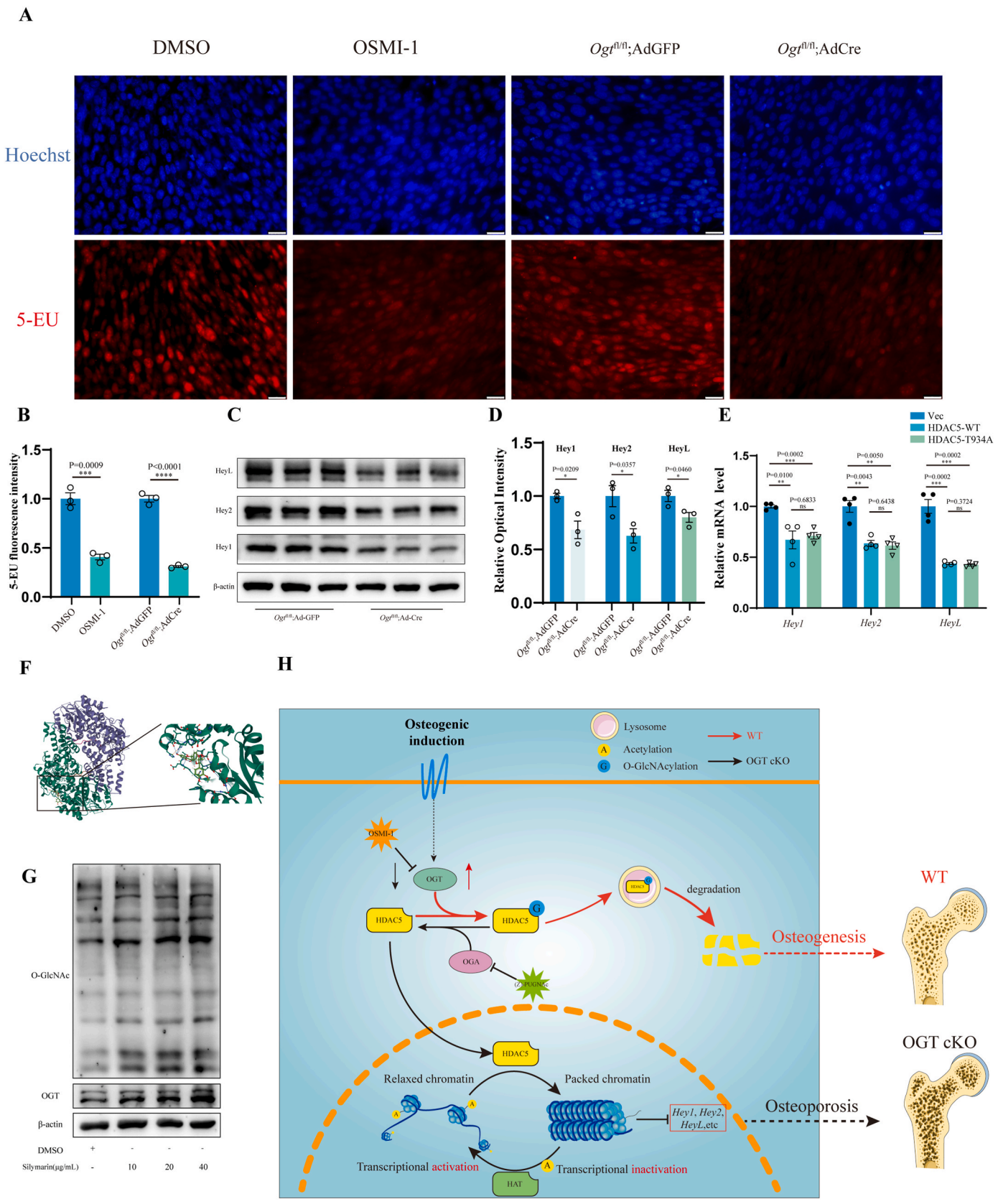


**Figure 8.** OGT deficiency elicits inhibition of Notch signaling in osteoblasts. **(A, B)** Fluorescence microscopy with nascent RNA in mBMSCs treated with OSMI-1 or in *Ogt* cKO mBMSCs (scale bars = 25 μm). **(C, D)** *Ogt* cKO decreased the protein levels of Hey1, Hey2 and HeyL. **(E)** mRNA levels of Hey1, Hey2, HeyL of C3H10T1/2 cells transfected with vectors, HDAC5-WT or HDAC5-T930A. **(F)**Molecular docking of silymarin-OGT complex. **(G)** The protein level of OGT by the treatment of silymarin. **(H)** Schematic illustration of this work. In WT mice, HDAC5 is O-GlcNAcylated by OGT, resulting in the proteolysis of HDAC5. In OGT cKO mice, HDAC5 cannot be O-GlcNAcylated and subsequent glycosylation-mediated degradation in the cytoplasm; instead, upon nuclear entry, it inhibits DNA transcription, consequently suppressing of osteogenesis. Data are represented as mean ± SEM. P-values are shown in the graphs.

osteogenesis, and is a positive regulator for osteogenesis. The OGT-mediated O-GlcNAcylation of HDAC5 modulates not only the nuclear/cytoplasmic ratio of HDAC5, but also the homeostasis between its cytoplasmic cleavage and nuclear entry, influencing the Notch signaling pathway and DNA epigenetic modifications, thereby contributing to osteogenesis (Fig. 8H). Our findings reveal an interaction between O-GlcNAcylation and acetylation and provide an innovative basis for elucidating the mechanism of osteogenesis. It also lays the foundation for the subsequent development of drugs for the treatment of osteoporosis, including small bioactive molecule silymarin.

## Authors' contributions

Y.D., X.G., C.L. and F.J.G. designed the study. Y.D., X.G., X.X.C., J.Q.C., H.L., L.L., Y.J. performed the experiments. X.G., L.H., Y.J., B.C.H. and Z.L.D analysed the data. Y.D., X.G., and F.J.G. prepared the manuscript. All authors contributed to the article and approved the submitted version.

## Availability of data and materials

The data and materials supporting the conclusions of this article are available upon request to the corresponding author.

## Declaration of competing interest

The authors declare that they have no known competing financial interests or personal relationships that could have appeared to influence the work reported in this paper.

## Acknowledgments

Funding: This study was funded by National Natural Science Foundation of China-The Youth Science Fund Project (No.82000836); Natural Science Foundation of Chongqing (CSTB2022NSCQ-MSX0066), The National Natural Science Foundation of China (No. 82272550, 82172386, 81922081), CQMU Program for Youth Innovation in Future Medicine (W0146). The Department of Education of Guangdong Province (2021KTSCX104), the Guangdong Basic and Applied Basic Research Foundation (2022A1515012164), and the Science, Technology, and Innovation Commission of Shenzhen (JCYJ20210324104201005).

## Appendix A. Supplementary data

Supplementary data to this article can be found online at https://doi.org/10.1016/j.jot.2024.10.004.

## References

[1] Qaseem A, Forciea MA, McLean RM, Denberg TD, Barry MJ, Cooke M, et al. Treatment of low bone density or osteoporosis to prevent fractures in men and women: a clinical practice guideline update from the American college of physicians. Ann Intern Med 2017;166:818–39. https://doi.org/10.7326/M15-1361.
[2] Clynes MA, Harvey NC, Curtis EM, Fuggle NR, Dennison EM, Cooper C. The epidemiology of osteoporosis. Br Med Bull 2020;133:105–17. https://doi.org/10.1093/bmb/ldaa005.
[3] Demontiero O, Vidal C, Duque G. Aging and bone loss: new insights for the clinician. Ther Adv Musculoskelet Dis 2012;4:61–76. https://doi.org/10.1177/1759720X11430858.
[4] Cosman F, Crittenden DB, Adachi JD, Binkley N, Czerwinski E, Ferrari S, et al. Romosozumab treatment in postmenopausal women with osteoporosis. N Engl J Med 2016;375:1532–43. https://doi.org/10.1056/NEJMoa1607948.
[5] Tsai JN, Lee H, David NL, Eastell R, Leder BZ. Combination denosumab and high dose teriparatide for postmenopausal osteoporosis (DATA-HD): a randomised, controlled phase 4 trial. Lancet Diabetes Endocrinol 2019;7:767–75. https://doi.org/10.1016/S2213-8587(19)30255-4.
[6] Leder BZ, Tsai JN, Uihlein AV, Wallace PM, Lee H, Neer RM, et al. Denosumab and teriparatide transitions in postmenopausal osteoporosis (the DATA-Switch study): extension of a randomised controlled trial. Lancet 2015;386:1147–55. https://doi.org/10.1016/S0140-6736(15)61120-5.
[7] Holt GD, Snow CM, Senior A, Haltiwanger RS, Gerace L, Hart GW. Nuclear pore complex glycoproteins contain cytoplasmically disposed O-linked N-acetylglucosamine. J Cell Biol 1987;104:1157–64. https://doi.org/10.1083/jcb.104.5.1157.
[8] Yang X, Qian K. Protein O-GlcNAcylation: emerging mechanisms and functions. Nat Rev Mol Cell Biol 2017;18:452–65. https://doi.org/10.1038/nrm.2017.22.
[9] Chatham JC, Zhang J, Wende AR. Role of O-linked N-acetylglucosamine protein modification in cellular (Patho)Physiology. Physiol Rev 2021;101:427–93. https://doi.org/10.1152/physrev.00043.2019.
[10] Hart GW, Housley MP, Slawson C. Cycling of O-linked beta-N-acetylglucosamine on nucleocytoplasmic proteins. Nature 2007;446:1017–22. https://doi.org/10.1038/nature05815.
[11] Hart GW, Slawson C, Ramirez-Correa G, Lagerlof O. Cross talk between O-GlcNAcylation and phosphorylation: roles in signaling, transcription, and chronic disease. Annu Rev Biochem 2011;80:825–58. https://doi.org/10.1146/annurev-biochem-060608-102511.
[12] Inoue D, Fujino T, Sheridan P, Zhang Y-Z, Nagase R, Horikawa S, et al. A novel ASXL1-OGT axis plays roles in H3K4 methylation and tumor suppression in myeloid malignancies. Leukemia 2018;32:1327–37. https://doi.org/10.1038/s41375-018-0083-3.
[13] Shin H, Leung A, Costello KR, Senapati P, Kato H, Moore RE, et al. Inhibition of DNMT1 methyltransferase activity via glucose-regulated O-GlcNAcylation alters the epigenome. Elife 2023;12. https://doi.org/10.7554/eLife.85595.
[14] Wang Y, Wang Y, Patel H, Chen J, Wang J, Chen Z-S, et al. Epigenetic modification of m6A regulator proteins in cancer. Mol Cancer 2023;22:102. https://doi.org/10.1186/s12943-023-01810-1.
[15] Koyama T, Kamemura K. Global increase in O-linked N-acetylglucosamine modification promotes osteoblast differentiation. Exp Cell Res 2015;338:194–202. https://doi.org/10.1016/j.yexcr.2015.08.009.
[16] Zhang Z, Huang Z, Awad M, Elsalanty M, Cray J, Ball LE, et al. O-GlcNAc glycosylation orchestrates fate decision and niche function of bone marrow stromal progenitors. Elife 2023;12. https://doi.org/10.7554/eLife.85464.
[17] McKinsey TA, Zhang CL, Lu J, Olson EN. Signal-dependent nuclear export of a histone deacetylase regulates muscle differentiation. Nature 2000;408:106–11. https://doi.org/10.1038/35040593.
[18] Lu J, McKinsey TA, Zhang CL, Olson EN. Regulation of skeletal myogenesis by association of the MEF2 transcription factor with class II histone deacetylases. Mol Cell 2000;6:233–44. https://doi.org/10.1016/s1097-2765(00)00025-3.
[19] Zhu H, Guo Z-K, Jiang X-X, Li H, Wang X-Y, Yao H-Y, et al. A protocol for isolation and culture of mesenchymal stem cells from mouse compact bone. Nat Protoc 2010;5:550–60. https://doi.org/10.1038/nprot.2009.238.
[20] Kurien BT, Scofield RH. Western blotting. Methods 2006;38:283–93. https://doi.org/10.1016/j.ymeth.2005.11.007.
[21] Weinreb C, Wolock S, Klein AM. SPRING: a kinetic interface for visualizing high dimensional single-cell expression data. Bioinformatics 2018;34:1246–8. https://doi.org/10.1093/bioinformatics/btx792.
[22] Xu Q, Yang C, Du Y, Chen Y, Liu H, Deng M, et al. AMPK regulates histone H2B O-GlcNAcylation. Nucleic Acids Res 2014;42:5594–604. https://doi.org/10.1093/nar/gku236.
[23] Wang Z, Li X, Yang J, Gong Y, Zhang H, Qiu X, et al. Single-cell RNA sequencing deconvolutes the in vivo heterogeneity of human bone marrow-derived mesenchymal stem cells. Int J Biol Sci 2021;17:4192–206. https://doi.org/10.7150/ijbs.61950.
[24] Wolock SL, Krishnan I, Tenen DE, Matkins V, Camacho V, Patel S, et al. Mapping distinct bone marrow niche populations and their differentiation paths. Cell Rep 2019;28:302–311.e305. https://doi.org/10.1016/j.celrep.2019.06.031.
[25] Trapnell C, Cacchiarelli D, Grimsby J, Pokharel P, Li S, Morse M, et al. The dynamics and regulators of cell fate decisions are revealed by pseudotemporal ordering of single cells. Nat Biotechnol 2014;32:381–6. https://doi.org/10.1038/nbt.2859.
[26] Ji Z, Ji H. TSCAN: pseudo-time reconstruction and evaluation in single-cell RNA-seq analysis. Nucleic Acids Res 2016;44:e117. https://doi.org/10.1093/nar/gkw430.
[27] Ortiz-Meoz RF, Jiang J, Lazarus MB, Orman M, Janetzko J, Fan C, et al. A small molecule that inhibits OGT activity in cells. ACS Chem Biol 2015;10:1392–7. https://doi.org/10.1021/acschembio.5b00004.
[28] Kim EJ, Perreira M, Thomas CJ, Hanover JA. An O-GlcNAcase-specific inhibitor and substrate engineered by the extension of the N-acetyl moiety. J Am Chem Soc 2006;128:4234–5. https://doi.org/10.1021/ja0582915.
[29] Zhou H, Zhang L, Chen Y, Zhu C-H, Chen F-M, Li A. Research progress on the hedgehog signalling pathway in regulating bone formation and homeostasis. Cell Prolif 2022;55:e13162. https://doi.org/10.1111/cpr.13162.
[30] Wang H, Yu H, Huang T, Wang B, Xiang L. Hippo-YAP/TAZ signaling in osteogenesis and macrophage polarization: therapeutic implications in bone defect repair. Genes Dis 2023;10:2528–39. https://doi.org/10.1016/j.gendis.2022.12.012.
[31] Peng Y, Wu S, Li Y, Crane JL. Type H blood vessels in bone modeling and remodeling. Theranostics 2020;10:426–36. https://doi.org/10.7150/thno.34126.
[32] Luo Z, Shang X, Zhang H, Wang G, Massey PA, Barton SR, et al. Notch signaling in osteogenesis, osteoclastogenesis, and angiogenesis. Am J Pathol 2019;189:1495–500. https://doi.org/10.1016/j.ajpath.2019.05.005.
[33] Zanotti S, Canalis E. Notch signaling and the skeleton. Endocr Rev 2016;37:223–53. https://doi.org/10.1210/er.2016-1002.

[34] Wein MN, Spatz J, Nishimori S, Doench J, Root D, Babij P, et al. HDAC5 controls MEF2C-driven sclerostin expression in osteocytes. J Bone Miner Res 2015;30:400–11. https://doi.org/10.1002/jbmr.2381.
[35] Tóth AD, Schell R, Lévay M, Vettel C, Theis P, Haslinger C, et al. Inflammation leads through PGE/EP(3) signaling to HDAC5/MEF2-dependent transcription in cardiac myocytes. EMBO Mol Med 2018;10. https://doi.org/10.15252/emmm.201708536.
[36] Rusilowicz-Jones EV, Urbé S, Clague MJ. Protein degradation on the global scale. Mol Cell 2022;82:1414–23. https://doi.org/10.1016/j.molcel.2022.02.027.
[37] Just S, Berger IM, Meder B, Backs J, Keller A, Marquart S, et al. Protein kinase D2 controls cardiac valve formation in zebrafish by regulating histone deacetylase 5 activity. Circulation 2011;124:324–34. https://doi.org/10.1161/CIRCULATIONAHA.110.003301.
[38] Chen J, Dong X, Cheng X, Zhu Q, Zhang J, Li Q, et al. Ogt controls neural stem/progenitor cell pool and adult neurogenesis through modulating Notch signaling. Cell Rep 2021;34:108905. https://doi.org/10.1016/j.celrep.2021.108905.
[39] Salhotra A, Shah HN, Levi B, Longaker MT. Mechanisms of bone development and repair. Nat Rev Mol Cell Biol 2020;21:696–711. https://doi.org/10.1038/s41580-020-00279-w.
[40] Benisch P, Schilling T, Klein-Hitpass L, Frey SP, Seefried L, Raaijmakers N, et al. The transcriptional profile of mesenchymal stem cell populations in primary osteoporosis is distinct and shows overexpression of osteogenic inhibitors. PLoS One 2012;7:e45142. https://doi.org/10.1371/journal.pone.0045142.
[41] Grabarics M, Lettow M, Kirschbaum C, Greis K, Manz C, Pagel K. Mass spectrometry-based techniques to elucidate the sugar code. Chem Rev 2022;122:7840–908. https://doi.org/10.1021/acs.chemrev.1c00380.
[42] Ye L, Ding W, Xiao D, Jia Y, Zhao Z, Ao X, et al. O-GlcNAcylation: cellular physiology and therapeutic target for human diseases. MedComm 2023;4(2020). https://doi.org/10.1002/mco2.456. e456.
[43] Bond MR, Hanover JA. A little sugar goes a long way: the cell biology of O-GlcNAc. J Cell Biol 2015;208:869–80. https://doi.org/10.1083/jcb.201501101.
[44] Bond MR, Hanover JA. O-GlcNAc cycling: a link between metabolism and chronic disease. Annu Rev Nutr 2013;33:205–29. https://doi.org/10.1146/annurev-nutr-071812-161240.
[45] Chang Y-H, Weng C-L, Lin K-I. O-GlcNAcylation and its role in the immune system. J Biomed Sci 2020;27:57. https://doi.org/10.1186/s12929-020-00648-9.
[46] Shi Q, Shen Q, Liu Y, Shi Y, Huang W, Wang X, et al. Increased glucose metabolism in TAMs fuels O-GlcNAcylation of lysosomal Cathepsin B to promote cancer metastasis and chemoresistance. Cancer Cell 2022;40. https://doi.org/10.1016/j.ccell.2022.08.012.
[47] Umapathi P, Mesubi OO, Banerjee PS, Abrol N, Wang Q, Luczak ED, et al. Excessive O-GlcNAcylation causes heart failure and sudden death. Circulation 2021;143:1687–703. https://doi.org/10.1161/CIRCULATIONAHA.120.051911.
[48] Lee BE, Suh P-G, Kim J-I. O-GlcNAcylation in health and neurodegenerative diseases. Exp Mol Med 2021;53:1674–82. https://doi.org/10.1038/s12276-021-00709-5.
[49] Li Y-N, Chen C-W, Trinh-Minh T, Zhu H, Matei A-E, Györfi A-H, et al. Dynamic changes in O-GlcNAcylation regulate osteoclast differentiation and bone loss via nucleoporin 153. Bone Res 2022;10:51. https://doi.org/10.1038/s41413-022-00218-9.
[50] Kim MJ, Kim HS, Lee S, Min KY, Choi WS, You JS. Hexosamine biosynthetic pathway-derived O-GlcNAcylation is critical for RANKL-mediated osteoclast differentiation. Int J Mol Sci 2021;22. https://doi.org/10.3390/ijms22168888.
[51] Taira TM, Ramos-Junior ES, Melo PH, Costa-Silva CC, Alteen MG, Vocadlo DJ, et al. HBP/O-GlcNAcylation metabolic Axis regulates bone resorption outcome. J Dent Res 2023;102:440–9. https://doi.org/10.1177/00220345221141043.
[52] Yang Y, Li X, Luan HH, Zhang B, Zhang K, Nam JH, et al. OGT suppresses S6K1-mediated macrophage inflammation and metabolic disturbance. Proc Natl Acad Sci U S A 2020;117:16616–25. https://doi.org/10.1073/pnas.1916121117.
[53] Takeuchi T, Horimoto Y, Oyama M, Nakatani S, Kobata K, Tamura M, et al. Osteoclast differentiation is suppressed by increased O-GlcNAcylation due to thiamet G treatment. Biol Pharm Bull 2020;43:1501–5. https://doi.org/10.1248/bpb.b20-00221.
[54] Qin W, Lv P, Fan X, Quan B, Zhu Y, Qin K, et al. Quantitative time-resolved chemoproteomics reveals that stable O-GlcNAc regulates box C/D snoRNP biogenesis. Proc Natl Acad Sci U S A 2017;114:E6749–58. https://doi.org/10.1073/pnas.1702688114.
[55] Yang Y, Yan Y, Yin J, Tang N, Wang K, Huang L, et al. O-GlcNAcylation of YTHDF2 promotes HBV-related hepatocellular carcinoma progression in an N6-methyladenosine-dependent manner. Signal Transduct Targeted Ther 2023;8:63. https://doi.org/10.1038/s41392-023-01316-8.
[56] Wu L, Cheng Y, Geng D, Fan Z, Lin B, Zhu Q, et al. O-GlcNAcylation regulates epidermal growth factor receptor intracellular trafficking and signaling. Proc Natl Acad Sci U S A 2022;119:e2107453119. https://doi.org/10.1073/pnas.2107453119.
[57] Zhang B, Li M-D, Yin R, Liu Y, Yang Y, Mitchell-Richards KA, et al. O-GlcNAc transferase suppresses necroptosis and liver fibrosis. JCI Insight 2019;4. https://doi.org/10.1172/jci.insight.127709.
[58] Huang H, Wu Q, Guo X, Huang T, Xie X, Wang L, et al. O-GlcNAcylation promotes the migratory ability of hepatocellular carcinoma cells via regulating FOXA2 stability and transcriptional activity. J Cell Physiol 2021;236:7491–503. https://doi.org/10.1002/jcp.30385.
[59] Sun Y, Zhang H, Qiu T, Liao L, Su X. Epigenetic regulation of mesenchymal stem cell aging through histone modifications. Genes Dis 2023;10:2443–56. https://doi.org/10.1016/j.gendis.2022.10.030.
[60] McIntyre RL, Daniels EG, Molenaars M, Houtkooper RH, Janssens GE. From molecular promise to preclinical results: HDAC inhibitors in the race for healthy aging drugs. EMBO Mol Med 2019;11:e9854. https://doi.org/10.15252/emmm.201809854.
[61] Bertogliat MJ, Morris-Blanco KC, Vemuganti R. Epigenetic mechanisms of neurodegenerative diseases and acute brain injury. Neurochem Int 2020;133:104642. https://doi.org/10.1016/j.neuint.2019.104642.
[62] Kong Y, Tannous P, Lu G, Berenji K, Rothermel BA, Olson EN, et al. Suppression of class I and II histone deacetylases blunts pressure-overload cardiac hypertrophy. Circulation 2006;113:2579–88. https://doi.org/10.1161/CIRCULATIONAHA.106.625467.
[63] Ohzono H, Hu Y, Nagira K, Kanaya H, Okubo N, Olmer M, et al. Targeting FoxO transcription factors with HDAC inhibitors for the treatment of osteoarthritis. Ann Rheum Dis 2023;82:262–71. https://doi.org/10.1136/ard-2021-221269.
[64] Majora M, Sondenheimer K, Knechten M, Uthe I, Esser C, Schiavi A, et al. HDAC inhibition improves autophagic and lysosomal function to prevent loss of subcutaneous fat in a mouse model of Cockayne syndrome. Sci Transl Med 2018;10. https://doi.org/10.1126/scitranslmed.aam7510.
[65] Rivadeneira F, Styrkársdottir U, Estrada K, Halldórsson BV, Hsu Y-H, Richards JB, et al. Twenty bone-mineral-density loci identified by large-scale meta-analysis of genome-wide association studies. Nat Genet 2009;41:1199–206. https://doi.org/10.1038/ng.446.
[66] Li H, Xie H, Liu W, Hu R, Huang B, Tan Y-F, et al. A novel microRNA targeting HDAC5 regulates osteoblast differentiation in mice and contributes to primary osteoporosis in humans. J Clin Invest 2009;119:3666–77. https://doi.org/10.1172/JCI39832.
[67] Jin F, Zhu Y, Liu M, Wang R, Cui Y, Wu Y, et al. Babam2 negatively regulates osteoclastogenesis by interacting with Hey1 to inhibit Nfatc1 transcription. Int J Biol Sci 2022;18:4482–96. https://doi.org/10.7150/ijbs.72487.
[68] Su X, Wei Y, Cao J, Wu X, Mou D, Luo J, et al. CCN3 and DLL1 co-regulate osteogenic differentiation of mouse embryonic fibroblasts in a Hey1-dependent manner. Cell Death Dis 2018;9:1188. https://doi.org/10.1038/s41419-018-1234-1.